Three-dimensional vibrometry of the human eardrum with stroboscopic lensless digital holography

Journal of Biomedical Optics

SPIEDigitalLibrary.org/jbo

Three-dimensional vibrometry of the human eardrum with stroboscopic lensless digital holography

Morteza Khaleghi
Cosme Furlong
Mike Ravicz
Jeffrey Tao Cheng
John J. Rosowski

SPIE

Three-dimensional vibrometry of the human eardrum with stroboscopic lensless digital holography

Morteza Khaleghi,[a,*] Cosme Furlong,[a,b,c] Mike Ravicz,[b,c] Jeffrey Tao Cheng,[b,c] and John J. Rosowski[b,c]
[a]Worcester Polytechnic Institute, Department of Mechanical Engineering, Center for Holographic Studies and Laser Micro-mechatronics, Worcester, Massachusetts 01609, United States
[b]Eaton-Peabody Laboratory, Massachusetts Eye and Ear Infirmary, Boston, Massachusetts 02114, United States
[c]Harvard Medical School, Department of Otology and Laryngology, Boston, Massachusetts 02114, United States

Abstract. The eardrum or tympanic membrane (TM) transforms acoustic energy at the ear canal into mechanical motions of the ossicles. The acousto-mechanical transformer behavior of the TM is determined by its shape, three-dimensional (3-D) motion, and mechanical properties. We have developed an optoelectronic holographic system to measure the shape and 3-D sound-induced displacements of the TM. The shape of the TM is measured with dual-wavelength holographic contouring using a tunable near IR laser source with a central wavelength of 780 nm. 3-D components of sound-induced displacements of the TM are measured with the method of multiple sensitivity vectors using stroboscopic holographic interferometry. To accurately obtain sensitivity vectors, a new technique is developed and used in which the sensitivity vectors are obtained from the images of a specular sphere that is being illuminated from different directions. Shape and 3-D acoustically induced displacement components of cadaveric human TMs at several excitation frequencies are measured at more than one million points on its surface. A numerical rotation matrix is used to rotate the original Euclidean coordinate of the measuring system in order to obtain in-plane and out-of-plane motion components. Results show that in-plane components of motion are much smaller (<20%) than the out-of-plane motions' components. [DOI: 10.1117/1.JBO.20.5.051028]

Keywords: 3-D displacement measurements; digital holography; holographic contouring; stroboscopic measurements; tympanic membrane.

Paper 140728SSR received Nov. 3, 2014; accepted for publication Dec. 31, 2014; published online Feb. 4, 2015.

1 Introduction

The hearing process involves a series of physical events in which acoustic waves in the outer ear are transduced into mechanical motions of the middle ear, acoustic and mechanical motions in the inner ear, and then into chemo-electro-mechanical reactions of the inner ear sensors that are interpreted by the brain.[1] Air in the ear canal has low mechanical impedance, whereas the mechanical impedance at the center of the eardrum, the umbo, is high. The eardrum or tympanic membrane (TM) must act as a transformer between these two impedances; otherwise, most of the energy will be reflected rather than transmitted.[2,3] The acousto-mechanical transformer behavior of the TM is determined by its shape, internal fibrous structure, and mechanical properties.[4–6] Therefore, full-field-of-view techniques are required to quantify shape, sound-induced displacements, and mechanical properties of the TM.[7–9] In our previous works,[10–12] we have reported holographic interferometric measurements of sound-induced displacements over a majority of the surface of mammalian TMs. A potential criticism of these measurements is that the displacements were measured only along one direction that was along the normal vector to the tympanic ring. Therefore, it was not possible to characterize all three-dimensional (3-D) motion components including those tangent (in-plane) and normal (out-of-plane) to the local plane of the TM. In this paper, developments of a single holographic system capable of measuring both shape with sub-millimeter resolution, and 3-D sound-induced motion of the TM with submicrometer resolution, are described. The accuracy and repeatability of the measuring system is tested and verified using artificial samples with geometries similar to those of human TMs. Then the system is used to measure the shape and 3-D sound-induced motions of human cadaveric TM samples at different tonal frequencies. Data obtained from the shape of the membrane are combined with the measured 3-D sound-induced motion components along three axes, x, y, and z, in order to obtain the motion's components tangent and normal to the local plane of the TM, enabling a more comprehensive view of TM mechanics.

*Address all correspondence to: Morteza Khaleghi, E-mail: mkm@wpi.edu

2 Methods

2.1 *Lensless Digital Holography*

In conventional holography, an optical lens is used to focus on an object of interest; however, our techniques are based on lensless digital holography in which reconstructions and focusing of the holograms are numerically obtained by Fresnel–Kirchhoff integrals.[13] Using temporal phase-stepping algorithms,[14,15] the complex amplitude of the hologram, $h(k,l)$, is obtained with

$$h(k,l) = [I_3(k,l) - I_1(k,l)] + i[I_4(k,l) - I_2(k,l)], \quad (1)$$

where I_1 to I_4 are intensity patterns of four consecutive phase-stepped frames of the camera with an induced phase step of $\pi/2$ between them, and k and l are the coordinates of the pixel in the CCD (hologram plane). As shown in Fig. 1, numerical reconstruction algorithms are based on two-dimensional (2-D)

Fast Fourier Transform (FFT) of the product of a reconstruction reference wave, $R(k,l)$, complex amplitude of the hologram, $h(k,l)$, and a chirp function, $\psi(k,l)$, that can be obtained with

$$\Gamma(m,n) = Q(m,n) \times \mathrm{FFT2}[R(k,l)h(k,l)\psi(k,l)], \tag{2}$$

where $\Gamma(m,n)$ is the complex reconstructed hologram at coordinates m and n in the reconstruction plane, $R(k,l)$ is the complex amplitude of the reference wave, $Q(m,n)$ and $\psi(k,l)$ are the quadratic phase factor and 2-D chirp function, respectively, and are defined by

$$Q(m,n) = \exp\left[-i\pi\lambda d\left(\frac{m^2}{N^2\Delta x^2} + \frac{n^2}{N^2\Delta y^2}\right)\right], \tag{3}$$

and

$$\psi(k,l) = \exp\left[\frac{-i\pi}{\lambda d}(k^2\Delta x^2 + l^2\Delta y^2)\right], \tag{4}$$

where Δx and Δy are the pixel size of the CCD sensor, N^2 is the number of pixels, λ is the laser wavelength, and d is the reconstruction distance. As shown in Fig. 1, the chirp function is a complex 2-D oscillatory signal, where the frequency of oscillation linearly varies with the spatial coordinate and is used for numerical reconstruction of the hologram at different distances of d. The reconstructed hologram, $\Gamma(m,n)$, is a complex function that contains both the amplitude and optical phase, $\varphi(m,n)$, that is defined by

$$\varphi(m,n) = \arg[\Gamma(m,n)]. \tag{5}$$

The fringe-locus function of a double-exposure (DE) hologram, i.e., the unwrapped optical phase difference of two reconstructed holograms corresponding to deformed and reference states of the object, is related to displacement with[15,16]

$$\Omega(m,n) = \mathrm{unwrap}(\varphi_{\mathrm{def}} - \varphi_{\mathrm{ref}}) = \frac{2\pi}{\lambda}\boldsymbol{K}\cdot\boldsymbol{d}(m,n), \tag{6}$$

where $\Omega(m,n)$ is the fringe-locus function at coordinates m and n in the reconstruction plane, φ_{def} and φ_{ref} are the optical phases of the reconstructed holograms recorded at deformed and reference states of the object, respectively, $\boldsymbol{K}(\boldsymbol{K}_x,\boldsymbol{K}_y,\boldsymbol{K}_z)$ is the sensitivity vector, defined by vectorial subtraction of the observation vector from the illumination vectors, and $\boldsymbol{d}(m,n)$ is the displacement vector with three components of $\boldsymbol{d}_x$, $\boldsymbol{d}_y$, and $\boldsymbol{d}_z$.

2.2 *Stroboscopic Measurements of Displacement*

Sound-induced vibrations of the TM are fast phenomena that require high-speed acquisition methods to be captured. In our system, we use stroboscopic measurements[17–21] with a conventional speed camera to capture the repetitive fast motions produced by sinusoidal stimuli. Acoustically induced motions of the TM are frozen at different stimulus phases using pulses of laser light to illuminate the sample at particular points during the sinusoidal excitation signal. As shown in Fig. 2, a dual-channel function generator is used with one of the channels set

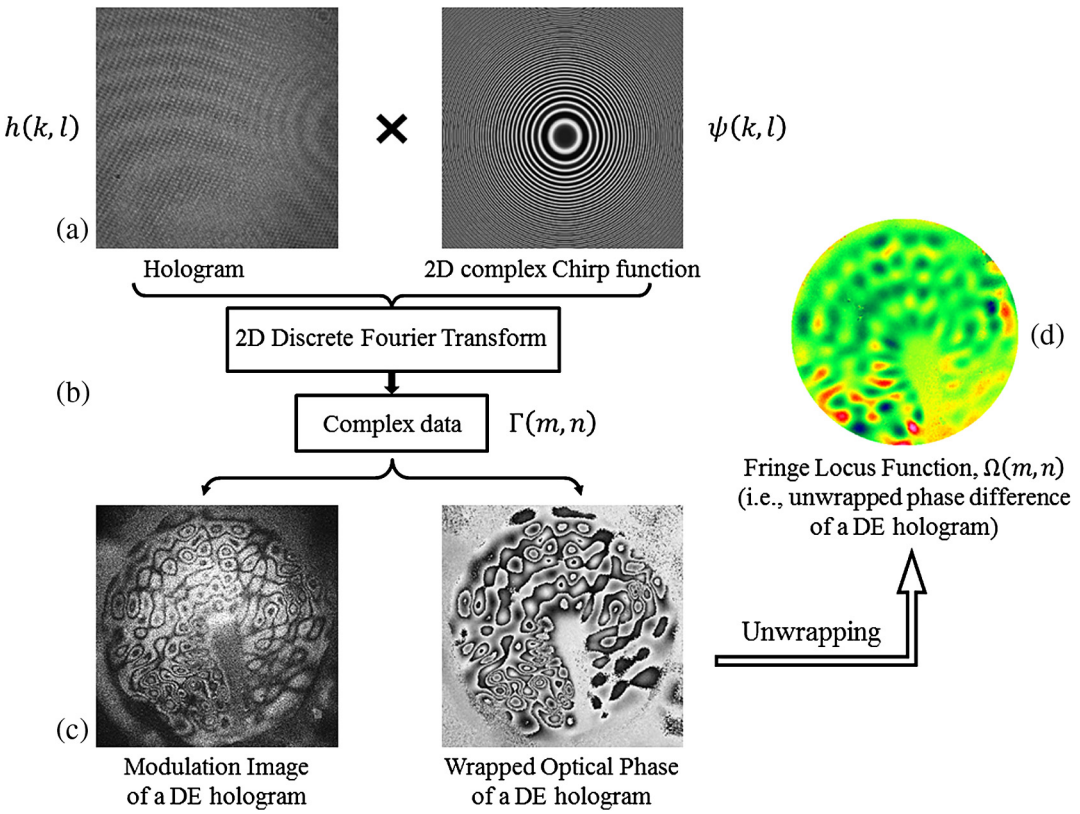

Fig. 1 Numerical algorithms used for reconstruction of digitally recorded holograms: (a) multiplication of complex amplitude of hologram, $h(k,l)$, with 2-D complex chirp function, $\psi(k,l)$, (b) numerical reconstruction of the hologram, $\Gamma(m,n)$, by 2-D FFT, (c) typical examples of modulation and wrapped optical phase of a reconstructed double-exposure (DE) hologram corresponding to sound-induced displacements of a TM sample, and (d) unwrapping the optical phase difference to obtain the fringe locus function, $\Omega(m,n)$.

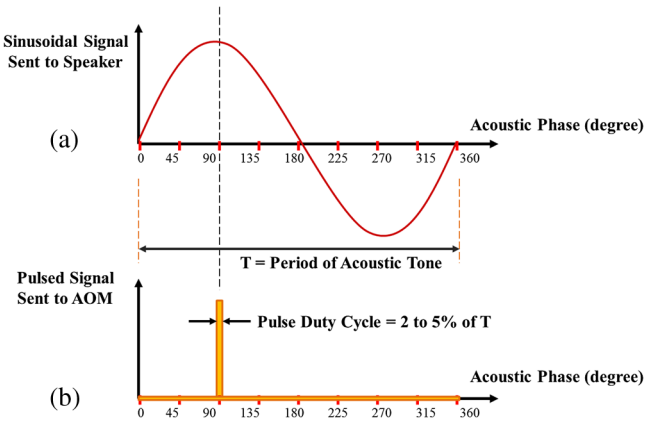

Fig. 2 Signals for stroboscopic measurements of sound-induced displacements of the TM at an example phase of 90 deg: (a) sinusoidal signal sent to the speaker to stimulate the TM and (b) pulsed signal sent to the acousto-optic modulator (AOM) that acts as a high-speed shutter for laser light illumination with a duty cycle of 2% to 5% of the tonal excitation period. During a full measurement, the phase position of the pulse is varied from 0 to 360 deg at specified increments to enable capturing of the entire cyclic motion.

to a sine wave for stimulating the TM through a speaker. The second channel is set to the same frequency but with a pulse wave to drive an acousto-optic modulator (AOM) to enable and disable the laser beam illumination. Typically, each laser pulse has a duration of 2% to 5% of the period of the tonal stimulus.[11,18] This generates the same effect as a strobe light by only capturing the motion of the TM at desired phases of the stimulus wave.

A DE technique that compares the deformed state strobe hologram gathered at one phase and a hologram gathered at a reference phase (usually 0) is used to compute the displacement of a series of strobe holograms to describe the phase-locked sound-induced variation in the optical phase. The result is a wrapped phase map that describes the differences in optical phase between the deformed and reference states. At every DE strobe hologram, including reference and deformed states, the system records four images containing holographic patterns that result from the phase stepping of the reference beam (RB) in steps of multiples of $\pi/2$. Considering the intensities at each pixel measured by the camera at each of the four phase steps to be $I_1, \ldots, I_4$ in the reference state, and $I'_1, \ldots, I'_4$ in the deformed state, the wrapped optical phase difference between any two states is related to displacements of the sample and is obtained with

$$\Delta\varphi(m,n) = \operatorname{atan2}\left[-\frac{(I_1-I_3)(I'_4-I'_2)-(I_4-I_2)(I'_1-I'_3)}{(I_1-I_3)(I'_1-I'_3)+(I_4-I_2)(I'_4-I'_2)}\right]. \tag{7}$$

2.3 *Dual-Wavelengths Shape Measurement*

The shape of the TM is measured with the method of dual-wavelength holographic contouring.[22,23] The technique requires acquisitions of a set of optical amplitude and phase information at wavelength λ_1, as well as a second set of amplitude and phase information at wavelength λ_2. As shown in Fig. 3, depth contours related to the shape of the object under investigation are defined by

$$\Delta\phi(m,n) = \phi_2 - \phi_1 = \frac{2\pi}{\Lambda}\mathrm{OPL}, \tag{8}$$

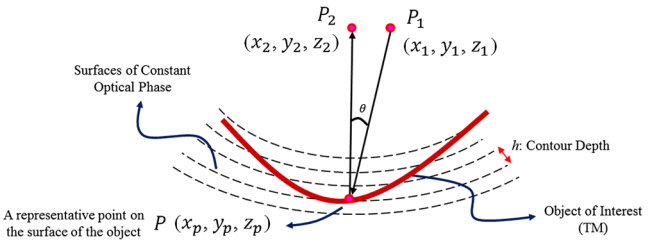

Fig. 3 Optical path length (OPL) of the laser light in dual-wavelength holographic contouring. P_1 is the point of illumination, P_2 is the point of observation, and P is a point on the surface of the object of interest. Surfaces of constant optical phase intersect the object of interest generating contours of depth h.

where ϕ_1 is the phase of the optical path length (OPL) recorded at the first wavelength λ_1, ϕ_2 is the phase of the OPL recorded at the second wavelength λ_2, and OPL is the OPL of the laser light from the point of illumination, (x_1, y_1, z_1), to a point on the surface of the object, (x_P, y_P, z_P), and to the point of observation, (x_2, y_2, z_2), and is defined with

$$\mathrm{OPL} = \sqrt{[(x_p-x_1)^2+(y_p-y_1)^2+(z_p-z_1)^2]}+\sqrt{[(x_2-x_p)^2+(y_2-y_p)^2+(z_2-z_p)^2]}. \tag{9}$$

The phase difference obtained with Eq. (8) is equivalent to performing measurements with a synthetic wavelength of Λ given by

$$\Lambda = \frac{\lambda_1\lambda_2}{|\lambda_1-\lambda_2|}, \tag{10}$$

which defines the contour depth, $h \approx (\Lambda/2)$.

In dual-wavelength contouring using phase-stepping algorithms, the phase difference, $\Delta\phi$, is a discontinuous wrapped function varying in the interval $[-\pi, \pi]$, thus phase unwrapping algorithms are applied to obtain a continuous phase distribution, $\Omega(m,n)$, for calculation of the relative height of each point on the surface of the object $Z(m,n)$ by

$$Z(m,n) = \frac{\Lambda}{2\pi[1+\cos(\theta)]}\Omega(m,n). \tag{11}$$

2.4 *3-D Displacement Measurements*

To ensure that measurements are reliable and independent of the measuring method, the holographic system is configured so that principal components of displacements, $\boldsymbol{d}_x$, $\boldsymbol{d}_y$, $\boldsymbol{d}_z$, can be measured with two different holographic interferometric approaches. The first one is based on the method of multiple illumination directions, whereas the second one uses a hybrid in-plane and out-of-plane displacement measurement method to obtain 3-D displacement data. In the hybrid method, in-plane measurements provide displacements' components along the x- and y-axes (perpendicular to the observation direction) and out-of-plane measurements provide displacements' components along the z-axis (along the observation direction).

2.4.1 *Method of multiple illumination directions*

Full field-of-view, 3-D, sound-induced displacements of the TM are measured with the method of multiple illumination

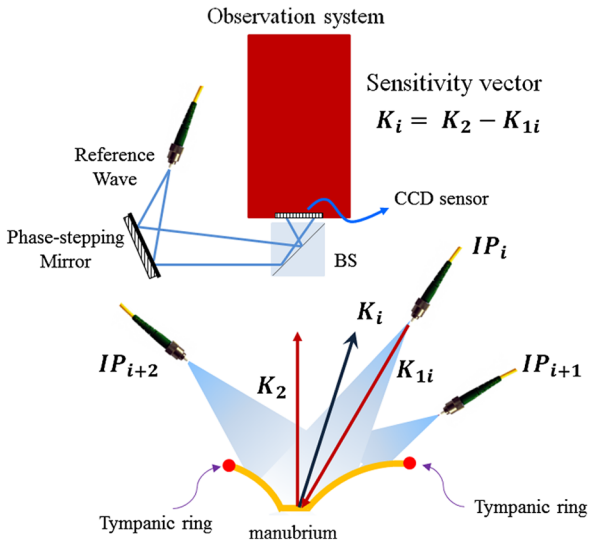

Fig. 4 3-D displacement measurements of the TM surface by the method of multiple illumination directions. Sensitivity vectors for each illumination direction, $\boldsymbol{K}_i$, are obtained by vectorial subtraction of the corresponding unit observation vector, $\boldsymbol{K}_2$, from the unit illumination vector, $\boldsymbol{K}_{1i}$. The geometry of the TM limits the maximum angle of illumination that can be implemented to achieve a well-conditioned sensitivity matrix.

directions in holographic interferometry.[24,25] In order to measure the three components of the displacement vector, $\boldsymbol{d}$, shown in Eq. (6), at least three independent measurements with different sensitivity vectors are required. In our approach, and to minimize experimental errors,[24,26] optical phase maps are obtained with four sensitivity vectors to form an over determined system of equations that is solved in Matlab with the least-squares error minimization method with

$$\{\boldsymbol{d}\} = [[\mathbb{S}]^T[\mathbb{S}]]^{-1} \times \{[\mathbb{S}]^T\{\Omega\}\}, \tag{12}$$

where $[\mathbb{S}]$ is the sensitivity matrix containing all the sensitivity vectors $\boldsymbol{K}_i$, shown in Fig. 4, and $\{\Omega\}$ is the fringe-locus function vector. In this method, all the sensitivity vectors need to be as linearly independent as possible for the system to provide accurate results. Therefore, the condition number, $\mathbb{C}$, of the square matrix, $[F] = [\mathbb{S}]^T[\mathbb{S}]$, characterizing the geometry of a holographic setup is calculated with[27]

$$\mathbb{C}(\mathbb{S}) = \sqrt{\frac{\lambda_{\max}(F)}{\lambda_{\min}(F)}}, \tag{13}$$

where $\lambda_{\max}$, and $\lambda_{\min}$ are the maximum and the minimum eigenvalues of $[F]$. A condition number close to one indicates a well-conditioned matrix, but this represents a holographic setup with large angles of illumination.[15,28] However, because of the particular cone-like geometry of the TM and the presence of the bony structures around it, as illustrated in Fig. 4, the maximum possible angles of illumination are limited. Therefore, a holographic setup has to be arranged to achieve the largest angles of illumination within the constraints imposed by the geometry of the TM. In this case, the condition number is greater than one, therefore, the accuracy of the measurements obtained with such a holographic setup has to be verified.

2.4.2 *Hybrid in-plane and out-of-plane method*

A hybrid method that utilizes independent and direct measurements of "out-of-plane" and "in-plane" displacements is used to test and verify the measurements obtained with the method of multiple sensitivity vectors. In this hybrid method, in-plane measurements provide displacement components along the x- and y-axes (perpendicular to the observation direction), and out-of-plane measurements provide displacements along the z-axis (along the observation direction), so that all three displacement components can be obtained independently.

Figure 5 shows optical configurations of the two measuring schemes. As shown in Fig. 5(a), an out-of-plane displacement d_{out} induces a change in the OPL of the laser light (OPD). Based on the geometry of the system, OPD is related to the out-of-plane displacement d_{out} with

$$\text{OPD} = d_{\text{out}}\cos(\theta_1), \tag{14}$$

where θ_1 is the angle between the illumination and observation directions. Using the wavenumber equation, $k = 2\pi/\lambda$, OPD is converted to the out-of-plane fringe-locus function, Ω_{out}, with $\Omega_{\text{out}} = (2\pi/\lambda)\text{OPD}$, and consequently, the out-of-plane displacement d_{out} is calculated with

$$d_{\text{out}} = \frac{\lambda\Omega_{\text{out}}}{2\pi[1+\cos(\theta_1)]}. \tag{15}$$

In the case of in-plane measurements, the object is illuminated with two symmetrical beams that interfere with each

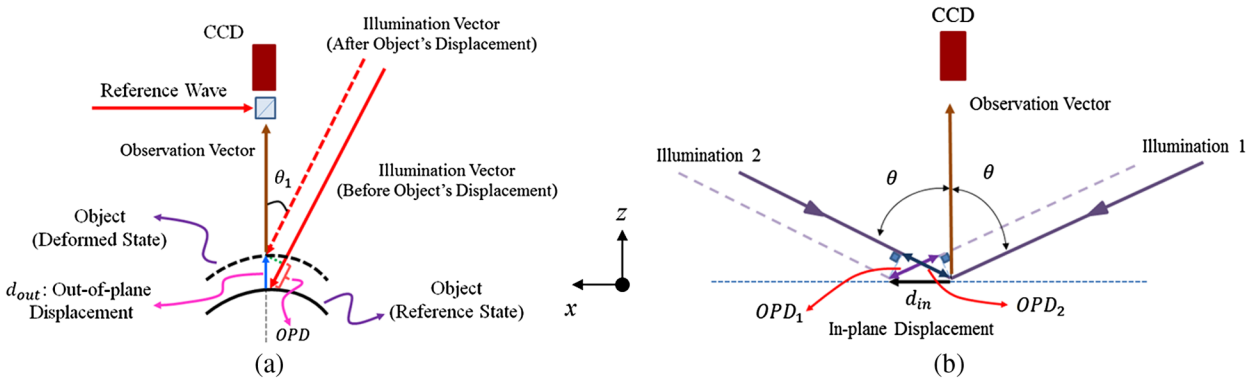

Fig. 5 Two displacement measurement schemes that are combined to achieve 3-D displacement measurements in the hybrid method: (a) configuration for out-of-plane (along z-axis) displacement measurements and (b) configuration for in-plane (along x- or y-axes) displacement measurements. The dashed lines represent illuminations after displacement occurs. OPD is OPL difference.

other and realize a self-reference configuration.[29] As shown in Fig. 5(b), once in-plane displacement, d_{in}, occurs, the OPL of each interfering beam changes, which causes a relative phase change between the two interfering beams. Figure 5(b) shows only one of the in-plane components of displacement, however, displacement components along both the x- and y-axes are independently measured with this method.

Equations (16) and (17) show the relation between OPD and the in-plane fringe-locus function corresponding to the in-plane displacement d_{in}

$$\mathrm{OPD}_1 = \mathrm{OPD}_2 = d_{in}\cos\left(\frac{\pi}{2} - \theta\right) = d_{in}\sin(\theta), \tag{16}$$

$$\Omega_{in} = \frac{2\pi}{\lambda}(\mathrm{OPD}_{total}), \tag{17}$$

where $\mathrm{OPD}_{total} = \mathrm{OPD}_1 + \mathrm{OPD}_2$. Using Eqs. (16) and (17), in-plane displacement, d_{in}, is calculated with

$$d_{in} = \frac{\lambda\Omega_{in}}{4\pi\sin(\theta)}, \tag{18}$$

where Ω_{in} is the in-plane fringe-locus Function, λ is the wavelength of the laser, and θ is the angle between the illumination and observation directions.

2.5 *Experimental Setup*

The schematic of the developed Digital Opto-Electronic Holographic System (DOEHS) is shown in Fig. 6. The DOEHS can measure microscale variations in shape as well as nanoscale displacements of the TM using both 3-D displacement measurement methods described in Sec. 2.4. The DOEHS consists of three main subsystems including laser delivery (LD), computing platform (CP), and optical head (OH). An external-cavity tunable diode laser capable of continuous tuning with minimal mode hopping (New Focus, Velocity) is placed in the LD, which provides a near IR laser light with a central wavelength of 780 nm. A polarization maintaining fiber coupler (Thorlabs PM-780-HP) splits the light into two beams to be used as reference (10%) and object (90%) beams. A MEMS optical switch, with a response time of less than 0.5 ms (Thorlabs OSW 8104), is used to multiplex between the object beams (OB) of each illumination direction once triggered by a Digital to Analog signal. The CCD is illuminated with the RB through a beam splitter and through a piezo-mounted mirror that is used for phase stepping. A 5 Megapixel (2452 × 2054 pixels) digital camera with a pixel pitch of 3.45 μm in the OH is used for image recording and the CP acquires and processes images in either time-averaged or DE stroboscopic modes.[30] The sinusoidal output of the function generator is amplified by a unity gain power amplifier and is used to drive the speaker. A microphone with a calibrated probe tube was positioned just at the edge of the TM to make measurements of sound pressure. In stroboscopic measurements, the light illumination is synchronized with the sound-waveform by means of a digital pulse signal from the function generator to the AOM.

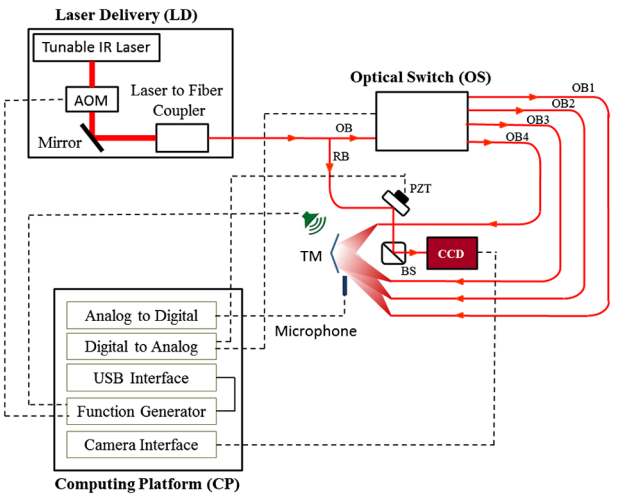

Fig. 6 Schematic of the developed holographic system for shape and 3-D displacement measurements. The laser delivery (LD) subsystem consists of a near-infrared tunable laser (with central wavelength of 780 nm), acousto-optic modulator (AOM), mirror, and laser to fiber coupler; the computing platform (CP) controls the recording parameter such as sound-excitation frequency and sound pressure level, phase-stepping, synchronizations for stroboscopic measurements, and controlling the optical switch (OS) for high-speed multiplexing between any of the object beams (OB1-OB4). The dashed lines are analog and digital signal lines.

2.6 *Determination of the Sensitivity Vectors*

In the method of multiple illumination directions, accurate determination of the position of each illumination source is required to define the corresponding sensitivity vectors. A new technique is developed in which all the sensitivity vectors are obtained by automatic analyses of the images of a specular sphere illuminated from different directions in order to avoid the uncertainties introduced by manual measurements. As shown in Fig. (7), a specular sphere is placed in front of the imaging system to acquire images from all four directions of illumination. The center of the image is marked in the acquisition software LaserView[30] and the sphere is accurately located in this position and within a circular mask provided by the software to ensure that the sphere is placed along the optical axis of the holographic system. As shown in Fig. 7(a), the mirror-like reflection creates a specular highlighted area on the sphere.[31] Each image is cropped and enhanced by image processing techniques that include histogram equalization, threshold definition, and edge detection. Then, a sphere is numerically fitted on the detected circular edge which represents the outline of the sphere. The normal vector of the fitted sphere at the centroid of the specular highlighted area, for each direction of illumination, defines the sensitivity vector, $\boldsymbol{K}_i$, which can be expressed as

$$\boldsymbol{K}_i = \boldsymbol{N}_x(x_{0i}, y_{0i}), \boldsymbol{N}_y(x_{0i}, y_{0i}), \boldsymbol{N}_z(x_{0i}, y_{0i}), \tag{19}$$

where $\boldsymbol{N}_x$, $\boldsymbol{N}_y$, and $\boldsymbol{N}_z$ are components of the unit normal vector, and (x_{0i}, y_{0i}) are the centroid coordinates of each of the specular highlighted areas. To accurately determine the centroids, (x_{0i}, y_{0i}), a circular Hough transform (CHT) algorithm is used. The Hough Transform can be used to determine the parameters of a circle when a number of points that fall on its perimeter are known.[32] A circle with radius R and center (x_0, y_0) can be described with the parametric equations

$$x = x_0 + R\cos(\theta), \tag{20}$$

$$y = y_0 + R\sin(\theta), \tag{21}$$

in which the angle θ sweeps through the full 360 deg range and the points (x, y) trace the perimeter of the circle. The output of

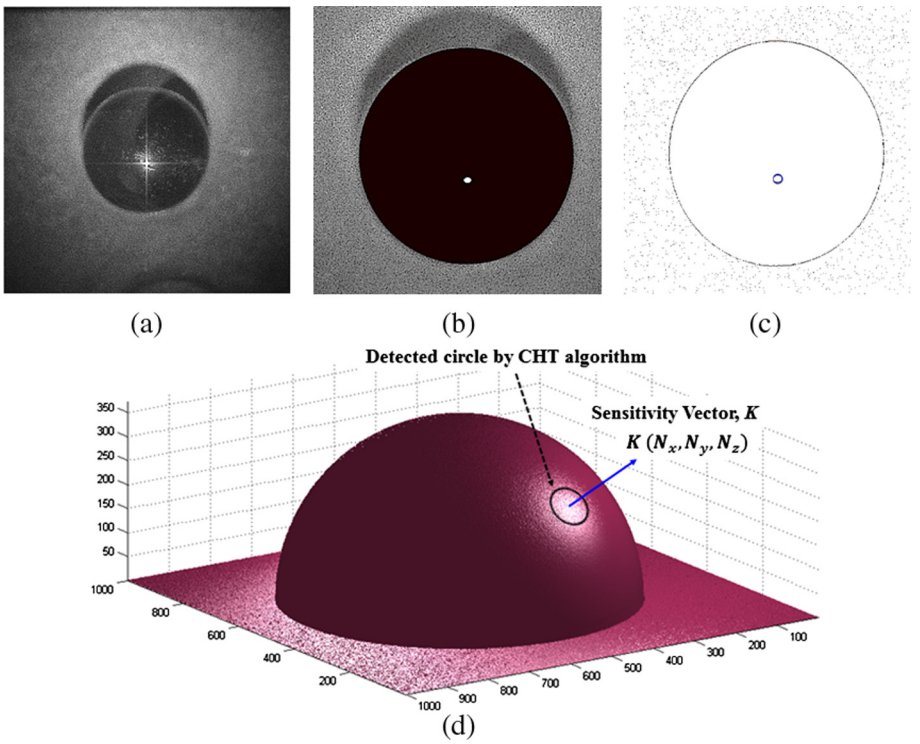

Fig. 7 Automatic determination of a sensitivity vector by use of a specular reflective sphere and circular Hough transformation (CHT): (a) image of a specular reflective sphere illuminated with one of the object beams, (b) cropped, enhanced image of the sphere, (c) CHT algorithm is used to detect the specular highlighted area and its centroid, and (d) the normal vector at the centroid of the detected highlighted area defines the sensitivity vector.

the CHT algorithm is the coordinate of the centroid of the specular highlighted area.

3 Results

3.1 *Validation of Measuring Accuracy and Repeatability*

Considering the acquisition speed of the 3-D holographic system and the time-dependent mechanical behavior of biological samples like the TM, we characterized the accuracy and repeatability of the measurements of the 3-D holographic system using measurements of artificial samples that have negligible time-varying behaviors. Based on the particular concave shape of the TM, a semispherical membrane with a geometry similar to the TMs is used. For 3-D displacement measurements of non-flat membranes, the large illumination angles necessary for a well-conditioned 3-D holographic system create shadows on the surface of the membrane. Therefore, the maximum angles of illumination are limited by geometrical constraints induced by the membrane, leaving the holographic system with condition numbers greater than one, as described in Sec. 2.4.1. To calibrate the measuring system and to verify the accuracy of the measurements obtained with such non-ideal 3-D holographic configuration, 3-D displacement components are measured using both of the methods described in Sec. 2.4, in order to ensure that the obtained displacement components are accurate and independent of the measuring approach. Once the accuracy of the measurements is verified, repeatability of the stroboscopic measurements is tested and verified with sound-induced displacement measurements of a latex membrane.

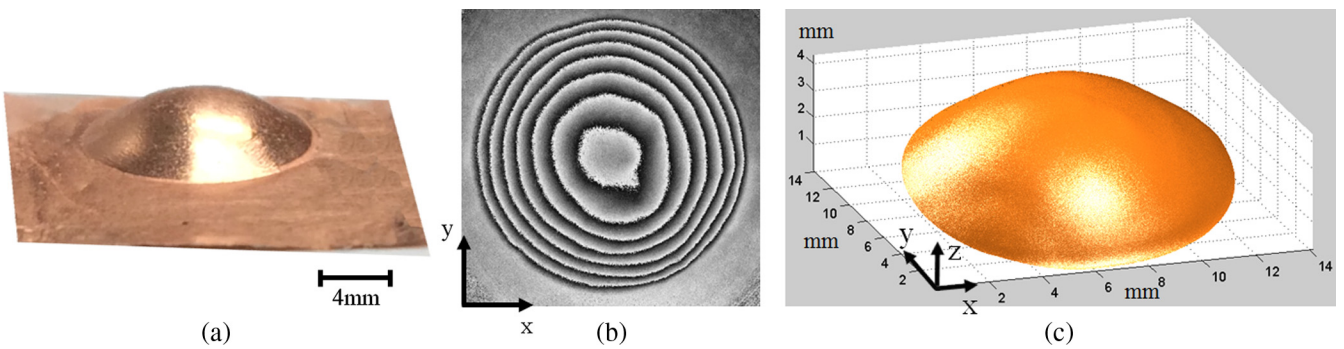

Fig. 8 Measurements of the shape of an artificial membrane using dual-wavelength holographic contouring: (a) semi-spherical membrane with a thickness of 25 μm and a radius of 6 mm, (b) wrapped optical phase corresponding to the shape of the membrane, and (c) 3-D scaled shape of the membrane.

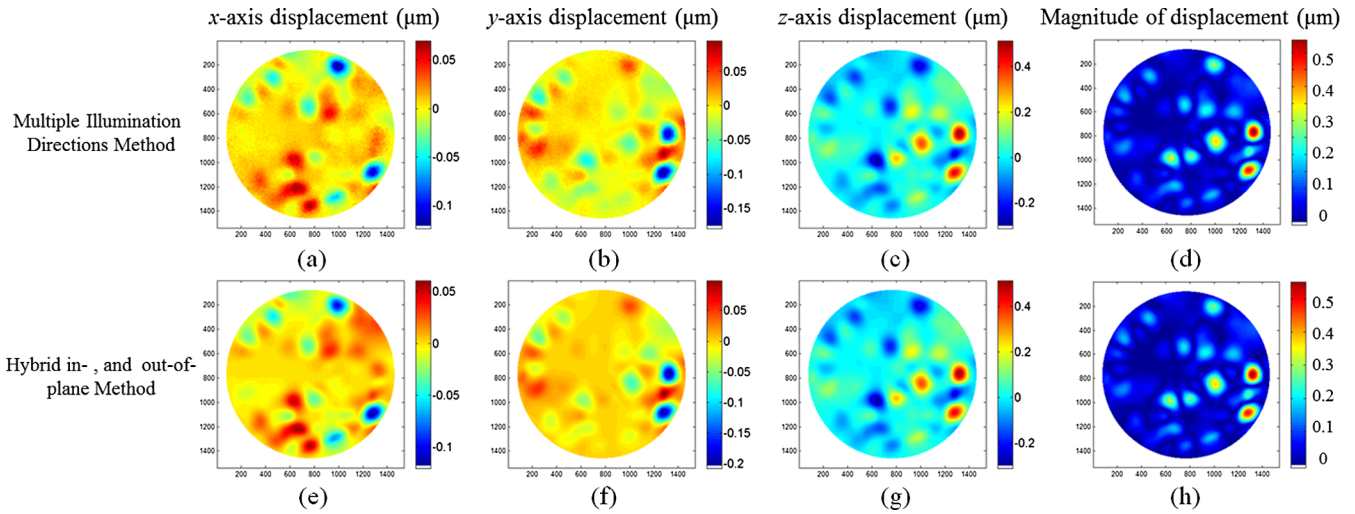

Fig. 9 3-D displacement components of a semi-spherical membrane excited mechanically with a piezoelectric shaker at a frequency of 25,418 Hz. Displacement components measured with the method of multiple illumination directions along (a) *x*-axis, (b) *y*-axis, (c) *z*-axis, (d) magnitude of displacement, and displacement components measured with the hybrid method along (e) *x*-axis, (f) *y*-axis, (g) *z*-axis, (h) magnitude of displacement. The correlation coefficient, $\mathbb{R}$, of the displacements component obtained with the two methods are 0.95, 0.96, 0.99, and 0.99 for displacement components along *x*-, *y*-, *z*-axes, and magnitude of displacement, respectively. All the displacements are in micrometers.

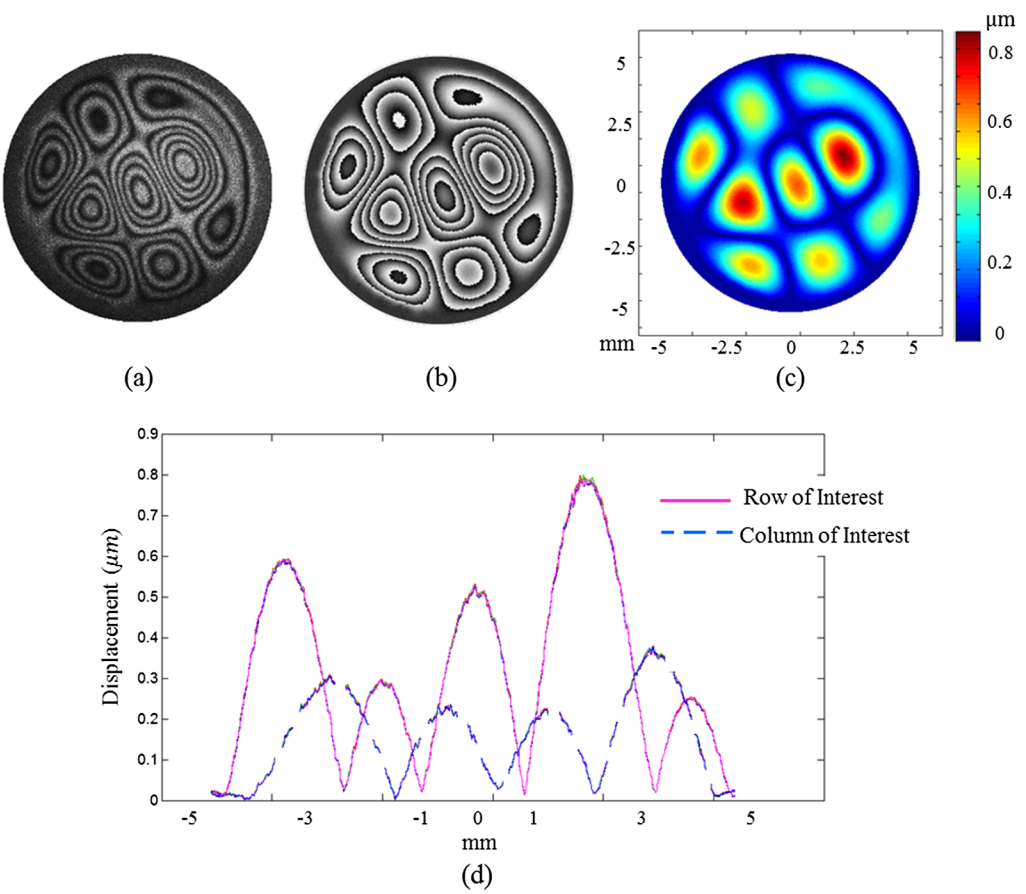

Fig. 10 Repeatability of the holographically obtained displacement measurements of a circular latex membrane acoustically excited with a tone of 2917 Hz at 91 dB SPL along one sensitivity vector. Representative DE (a) modulation, (b) wrapped optical phase, (c) map of the magnitudes of displacements averaged over six consecutive measurements, and (d) cross-sections of six displacement maps along specific horizontal (solid) and vertical lines (dashed), illustrating the repeatability of the measurements.

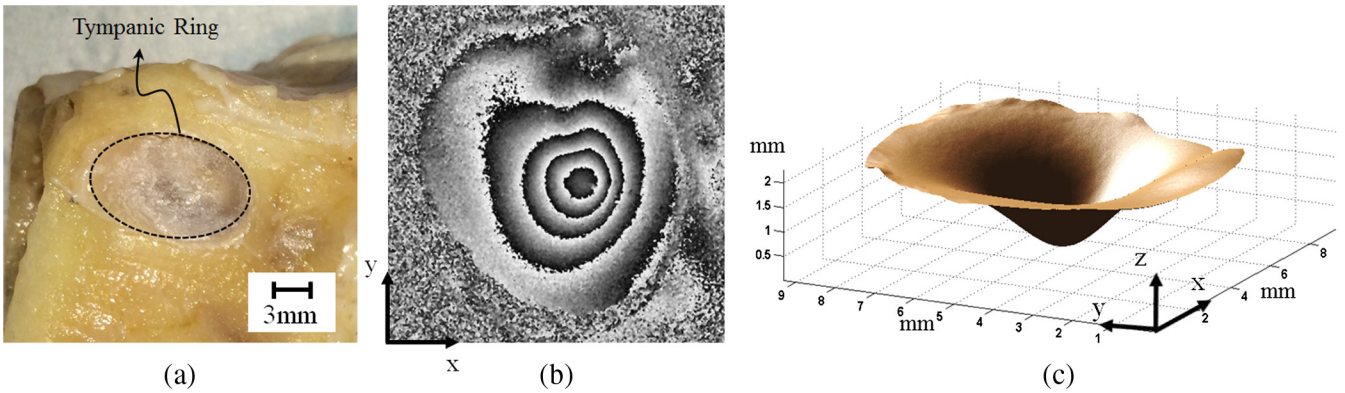

Fig. 11 Measuring the shape of a human tympanic membrane (TM) using dual-wavelength holographic contouring: (a) human temporal bone highlighting the tympanic ring, (b) wrapped optical phase corresponding to the shape of the TM, and (c) 3-D shape of the TM. The shape is measured with wavelengths of 780.2 and 780.6 nm.

3.1.1 *Accuracy of 3-D displacement measurements*

The shape and 3-D displacements of a thin semispherical membrane, shown in Fig. 8, with a radius of 6 mm and a thickness of 25 μm are measured with the developed holographic system. The shape of the membrane is measured with a dual-wavelength contouring method with wavelengths of 779.8 and 780.6 nm. Figure 8(b) shows the wrapped optical phase, which is unwrapped and scaled to obtain the corresponding 3-D shape, as shown in Fig. 8(c).

The semispherical membrane is mounted on a piezoelectric shaker (JODON EV-100) that can operate at frequencies as high as 150 kHz. By sweeping the excitation frequency and

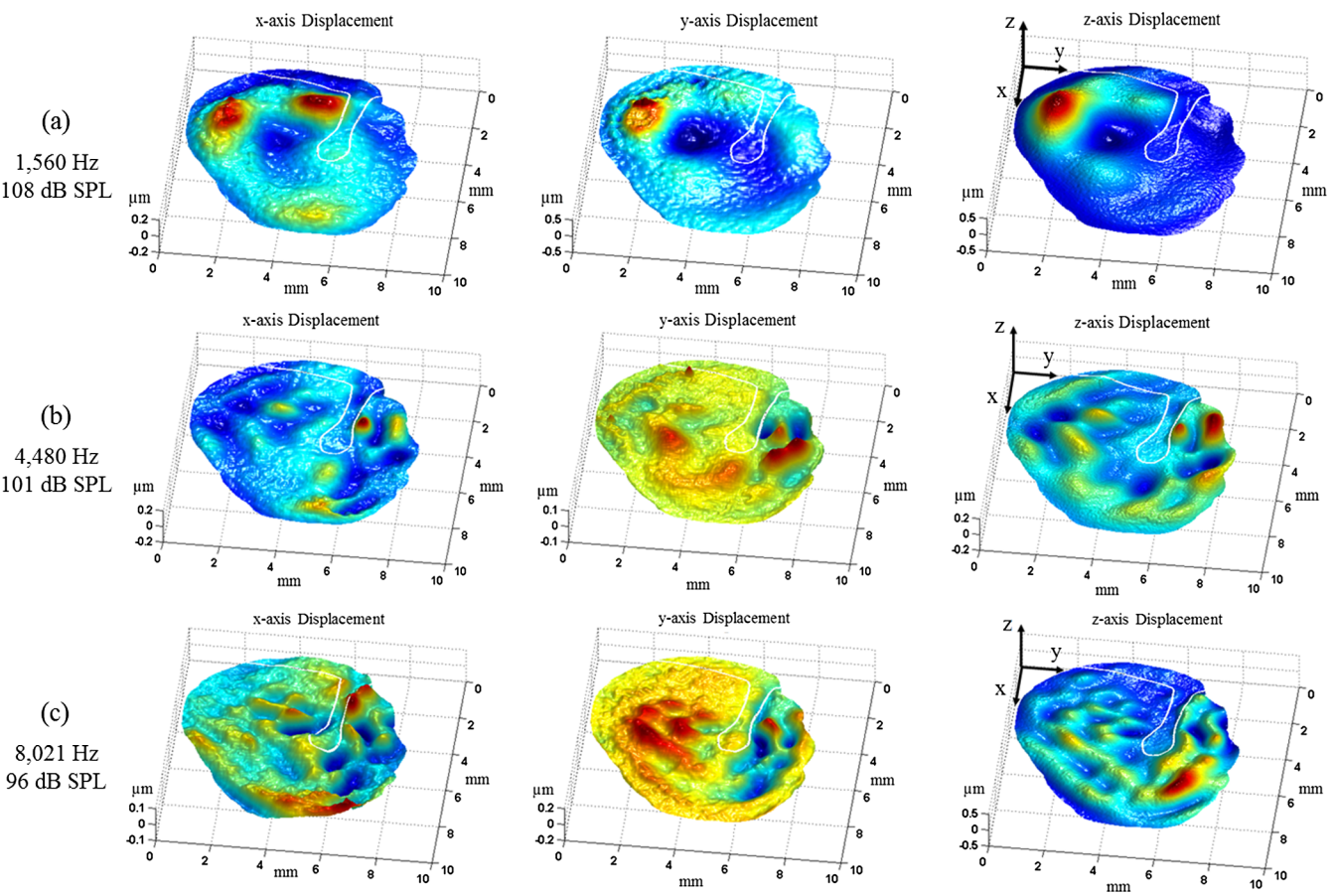

Fig. 12 Measured 3-D sound-induced displacement of a human TM along the *x*-, *y*-, and *z*-axes at three different tonal excitations. Magnitudes of displacements along *x*-, *y*-, and *z*-axes are (a) ±220, ±250, and ±520 nm for tonal frequency of 1560 Hz at 108 dB SPL, (b) ±200, ±120, and ±220 nm for tonal frequency of 4480 Hz at 101 dB SPL, and (c) ±110, ±210, and ±510 nm for tonal frequency of 8021 Hz at 96 dB SPL. The diameter of the TM is 8 mm and the outline shows the handle of malleus (manubrium).

monitoring the membrane's time-averaged motions,[10,16,33] an appropriate mode of vibration is chosen. Representative results are shown in Fig. 9, in which the membrane is excited with a frequency of 25,418 Hz and amplitude of 0.4 V. Comparisons of the displacement components along the x-, y-, z-axes, and the magnitudes of displacements obtained with both methods show correlation coefficients >95%, illustrating that the measurements are accurate, repeatable, and independent of the measuring method.

3.1.2 *Repeatability of stroboscopic measurements*

Repeatability of the results obtained with the 3-D holographic system is tested and verified by a series of consecutive stroboscopic measurements of a 10 mm diameter latex membrane excited with a tone of 2917 Hz at 91 dB sound pressure level (SPL), as shown in Fig. 10. Figures 10(a)–10(c) show representative examples of the obtained modulation, wrapped optical phase, and magnitude of displacements, respectively. Furthermore, repeatability of the measurements is shown in Fig. 10(d), where vertical (shown with dashed lines) and horizontal (shown with solid lines) cross-sections of six consecutive displacement measurements lie on top of each other.

3.2 *Shape and 3-D Sound-Induced Displacements of Human TM*

The TM sample was part of a human right ear temporal bone from a 49-year-old male donor. The sample was prepared in accordance with previously established procedures.[9,12] In order to have the least amount of shadow on the surface of the TM, all the bony structures around the TM were removed. In preparing the specimen, it was necessary to also open the middle ear cavity, however, those openings were filled by silicone impression materials (Westone Inc.) prior to these measurements in order to avoid and minimize the air flow through the middle ear cavity. Also, to enhance light reflection from the sample and to reduce the required camera exposure time in order to have a better signal to noise ratio, the lateral surface of the TM was coated with a solution of zinc oxide. The effect of this coating on the vibrational patterns of the TM has been shown to be negligible.[9–11] The shape of the sample was measured with dual-wavelength holographic contouring, as shown in Fig. 11, with two wavelengths of 780.2 and 780.6 nm. Figure 11(b) shows the wrapped optical phase, which is unwrapped and scaled to obtain corresponding 3-D shape, as shown in Fig. 11(c).

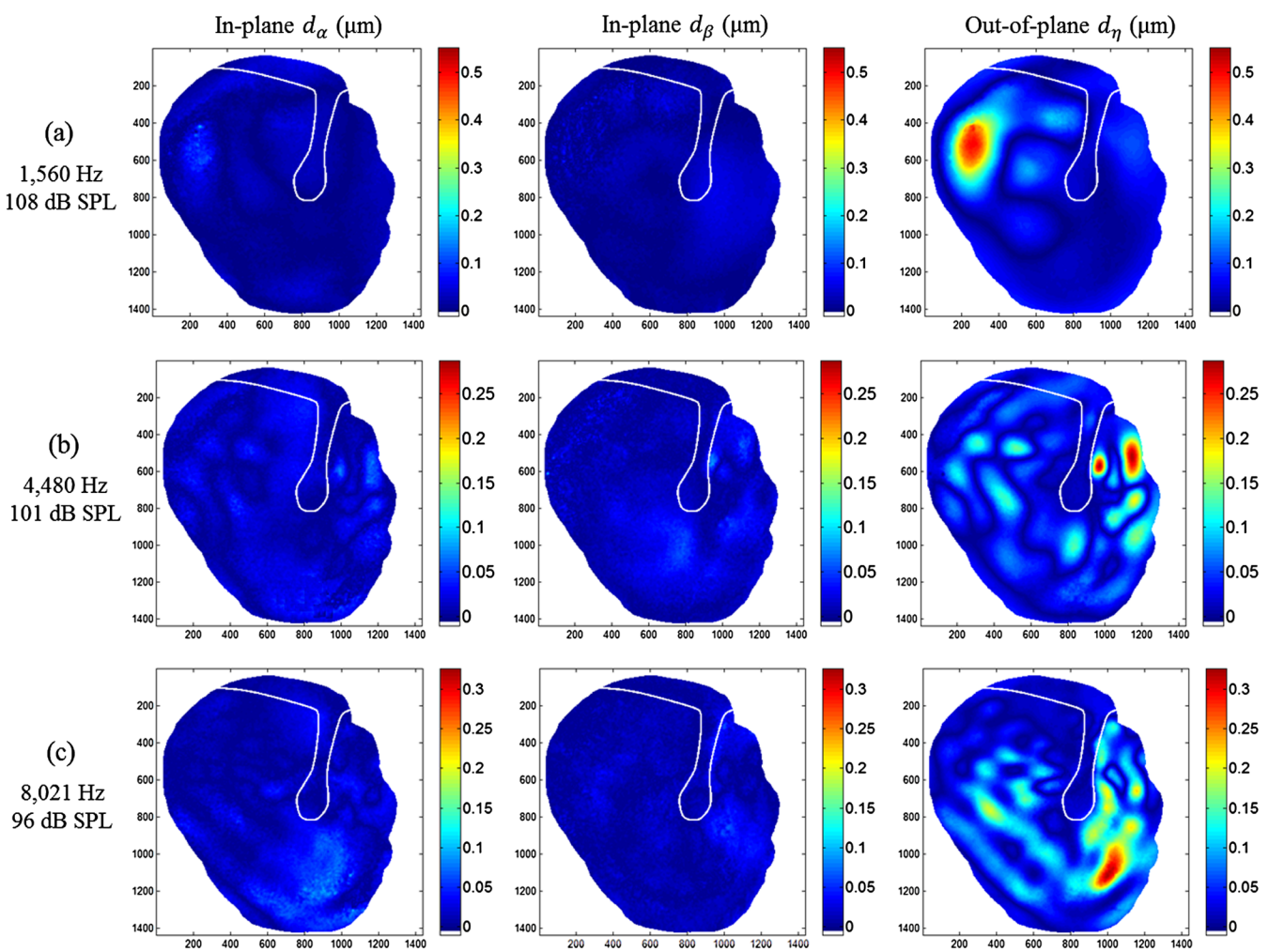

Fig. 13 In-plane and out-of-plane sound-induced motions of a human TM excited with frequency of (a) 1560 Hz at 108 dB SPL, (b) 4480 Hz at 101 dB SPL, and (c) 8021 Hz at 96 dB SPL. It can be clearly seen that tangential (in-plane) components are negligible and the motions are mainly normal (out-of-plane) to the TM surface. Displacements are in the unit of micrometers.

Tones with different frequencies were used to stimulate the membrane and 3-D sound-induced displacement components of the surface of the TM were acquired. Figure 12 shows 3-D displacement components of the TM along the x-, y-, and z-axes produced by tones of 1560 Hz at 108 dB SPL, 4480 Hz at 101 dB SPL, and 8021 Hz at 96 dB SPL. The levels were selected to generate measurable sound-induced TM displacements. As shown in Fig. 12, as sound excitation frequency increases, the number of local maxima in the displacement patterns also increases and sound-induced motion patterns of the TM become more complex.

Combining data obtained from the shape of the membrane, shown in Fig. 11, with measured 3-D sound-induced displacement components, shown in Fig. 12, displacement components tangent (in-plane) and normal (out-of-plane) to the TM surface are obtained. A numerical rotation matrix is used[34] to rotate the original Euclidean coordinate system of the measuring system (x, y, z), so that the new coordinate system (α, β, η) has unit vectors tangent and normal to the TM surface. Figure 13 shows the results of the rotation of the coordinate system, where rotated displacements have components tangent (in-plane components d_α and d_β), and normal to the TM surface (out-of-plane component d_η). As shown in this figure, in-plane components are much smaller than out-of-plane components (<20%), so that the displacement vectors can be considered to be mainly normal to the surface of the TM.

These data support hypotheses based on considering the motions of the TM similar to those of thin-shells, in which the tangential motions' components are negligible and the motion vectors are hypothesized to be mainly along the normal vector of the surface of the membrane.[8,9]

4 Conclusions

While there are many hypotheses of how the TM couples sound to the rest of the ear, there is little data to support them.[2,3,8] Knowledge about the shape and 3-D sound-induced displacement of the TM are necessary sets of data in order to better understand the acousto-mechanical transformer behavior of the mammalian TMs. In this direction, we are developing opto-electronic holographic systems capable of measuring shape with sub-millimeter resolution, and 3-D sound-induced displacement of the TM with sub-micrometer resolution. Combining the measured shape and 3-D sound-induced displacements of the TM at each point on its surface enables characterization of the motion's components tangent and normal to the TM surface. Results show that the tangential motions' components are much smaller (<20%) than the out-of-plane motions' components. These results are consistent with the modeling of mammalian TM as thin-shells in which the tangential motions' components are negligible.

Appendix: Rotation Matrix used to Obtain In-Plane and Out-of-Plane Displacements

The original Euclidean coordinate system x, y, z is mathematically rotated in order to obtain the local in-plane and out-of-plane displacement components. In the holographic system and based on the definition of the sensitivity vectors, the observation vector $\boldsymbol{Z}$, i.e., a vector perpendicular to the CCD sensor, has unit vector components Z_x, Z_y, and Z_z equal to [0, 0, 1]. Also, by having the 3D shape of the membrane, the unit normal vector, $\boldsymbol{N}$, at every point on the surface of the TM is quantified. Since, both $\boldsymbol{N}$ and $\boldsymbol{Z}$ are unit vectors, the angle between them is calculated with dot product of the two vectors; and the cross product of these two vectors provide a vector, $\boldsymbol{U}$, normal to both of them that, in this case, is tangent to the local plane of the membrane and is considered as the axis of rotation.

The rotation matrix R, is used to rotate the original displacement vector $\boldsymbol{d}(\boldsymbol{d}_x, \boldsymbol{d}_y, \boldsymbol{d}_z)$, based on the rotation angle θ and the unit vector of the axis of rotation $\boldsymbol{U}$ with

$$R = \begin{bmatrix} \cos\theta + \boldsymbol{U}_1^2(1-\cos\theta) & \boldsymbol{U}_1\boldsymbol{U}_2(1-\cos\theta) - \boldsymbol{U}_3\sin\theta & \boldsymbol{U}_1\boldsymbol{U}_3(1-\cos\theta) + \boldsymbol{U}_2\sin\theta \\ \boldsymbol{U}_2\boldsymbol{U}_1(1-\cos\theta) + \boldsymbol{U}_3\sin\theta & \cos\theta + \boldsymbol{U}_2^2(1-\cos\theta) & \boldsymbol{U}_2\boldsymbol{U}_3(1-\cos\theta) - \boldsymbol{U}_1\sin\theta \\ \boldsymbol{U}_3\boldsymbol{U}_1(1-\cos\theta) - \boldsymbol{U}_2\sin\theta & \boldsymbol{U}_3\boldsymbol{U}_2(1-\cos\theta) + \boldsymbol{U}_1\sin\theta & \cos\theta + \boldsymbol{U}_3^2(1-\cos\theta) \end{bmatrix} \quad (22)$$

where $\boldsymbol{U} = (\boldsymbol{U}_1, \boldsymbol{U}_2, \boldsymbol{U}_3)$ is the unit vector of the axis of rotation of the observation direction (z-axis in the original measuring coordinate system), and θ is the angle of rotation. Therefore, as shown in Fig. 14, at each point m, n, the rotated displacement vector $\boldsymbol{d}_{\text{rot}}$ has components tangent ($\boldsymbol{d}_\alpha$ and $\boldsymbol{d}_\beta$) and normal ($\boldsymbol{d}_\eta$) to the local TM plane and is calculated with the matrix multiplication of the rotation matrix, R, with the original displacement vector $\boldsymbol{d}$ with

$$\boldsymbol{d}_{\text{rot}}(m, n) = R \times \boldsymbol{d}(m, n). \quad (23)$$

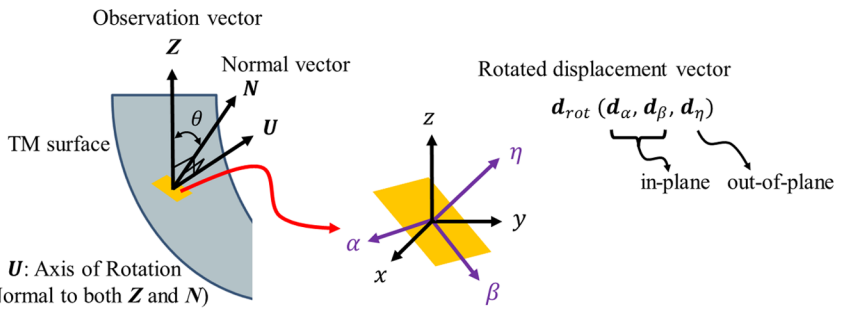

Fig. 14 Transformation of the global measuring coordinate system x, y, z to the local coordinate system α, β, η, of the TM. The observation vector $\boldsymbol{Z}$ is rotated θ degrees along the axis of rotation $\boldsymbol{U}$.

Acknowledgments

This work was supported by the National Institute on Deafness and other Communication Disorders (NIDCD), the National Institutes of Health (NIH), Massachusetts Eye and Ear Infirmary (MEEI), and Mechanical Engineering Department at Worcester Polytechnic Institute. We also acknowledge the support of all of the members of the CHSLT labs at WPI and Eaton-Peabody labs at MEEI, in particular Ellery Harrington and Ivo Dobrev.

References

1. C. D. Geisler, *From Sound to Synapse: Physiology of the Mammalian Ear*, Oxford University Press, New York (1998).
2. S. Puria and C. Steele, "Tympanic-membrane and malleus–incus-complex co-adaptations for high-frequency hearing in mammals," *Hear. Res.* **263**(1), 183–190 (2010).
3. R. Z. Gan et al., "Finite element modeling of sound transmission with perforations of tympanic membrane," *J. Acoust. Soc. Am.* **126**(1), 243–253 (2009).
4. O. Rochefoucauld and E. S. Olson, "A sum of simple and complex motions on the eardrum and manubrium in gerbil," *Hear. Res.* **263**(1), 9–15 (2010).
5. J. P. Fay, S. Puria, and C. R. Steele, "The discordant eardrum," *Proc. Natl Acad. Sci.* **103**(52), 19743–19748 (2006).
6. X. Zhang et al., "Experimental and modeling study of human tympanic membrane motion in the presence of middle ear liquid," *J. Assoc. Res. Otolaryngol.* **15**(6), 867–881 (2014).
7. J. Tonndorf and S. M. Khanna, "Tympanic-membrane vibrations in human cadaver ears studied by time-averaged holography," *J. Acoust. Soc. Am.* **57**(4B), 1221–1233 (1972).
8. W. F. Decraemer and W. R. J. Funnell, "Anatomical and mechanical properties of the tympanic membrane," in *Chronic Otitis Media. Pathogenesis-Oriented Therapeutic Management*, B. Ars, Eds., pp. 51–84, Kugler Publications, Amsterdam, The Netherlands (2008).
9. J. J. Rosowski et al., "Measurements of three-dimensional shape and sound-induced motion of the chinchilla tympanic membrane," *Hear. Res.* **301**, 44–52 (2013).
10. J. J. Rosowski et al., "Computer-assisted time-averaged holography of the motion of the surface of the tympanic membrane with sound stimuli of 0.4 to 25 kHz," *Hear. Res.* **253**(1–2), 83–96 (2009).
11. J. M. Flores-Moreno et al., "Holographic otoscope for nanodisplacement measurements of surfaces under dynamic excitation," *Scanning* **33**(5), 342–352 (2011).
12. J. T. Cheng et al., "Motion of the surface of the human tympanic membrane measured with stroboscopic holography," *Hear Res.* **263**, 66–77 (2010).
13. U. Schnars et al., *Digital Holography and Wavefront Sensing*, pp. 39–68, Springer, Berlin, Heidelberg (2015).
14. I. Yamaguchi and T. Zhang, "Phase-shifting digital holography," *Opt. Lett.* **22**(16), 1268–1270 (1997).
15. C. M. Vest, *Holographic Interferometry*, John Wiley and Sons, Inc., New York (1979).
16. R. J. Pryputniewicz, "Time average holography in vibration analysis," *Opt. Eng.* **24**(5), 245843 (1985).
17. D. De Greef et al., "Viscoelastic properties of the human tympanic membrane studied with stroboscopic holography and finite element modeling," *Hear. Res.* **312**, 69–80 (2014).
18. M. Khaleghi et al., "Digital holographic measurements of shape and three-dimensional sound-induced displacements of tympanic membrane," *Opt. Eng.* **52**(10), 101916 (2013).
19. J. Leval et al., "Full-field vibrometry with digital Fresnel holography," *App. Opt.* **44**(27), 5763–5772 (2005).
20. G. Pedrini, W. Osten, and M. E. Gusev, "High-speed digital holographic interferometry for vibration measurement," *App. Opt.* **45**(15), 3456–3462 (2006).
21. M. S. Hernández-Montes et al., "Digital holographic interferometry applied to the study of tympanic membrane displacements," *Opt. Laser Eng.* **49**(6), 698–702 (2011).
22. C. Furlong and R. J. Pryputniewicz, "Absolute shape measurements using high-resolution optoelectronic holography methods," *Opt. Eng.* **39**(1), 216–223 (2000).
23. P. Bergström et al., "Shape verification using dual-wavelength holographic interferometry," *Opt. Eng.* **50**(10), 101503 (2011).
24. T. Kreis, *Handbook of Holographic Interferometry*, Wiley-VCH Verlag GmbH & Co. KGaA, Weinheim, Germany (2005).
25. W. F. Decraemer et al., "Three-dimensional vibration of the malleus and incus in the living gerbil," *J. Assoc. Res. Otolaryngol.* **15**, 483–510 (2014).
26. A. Alamdari et al., "Kinetostatic optimization for an adjustable four-bar based articulated leg-wheel subsystem," in *IEEE International Conference on Intelligent Robots and Systems (IROS 2014)*, pp. 2860–2866, IEEE, Piscataway, New Jersey (2014).
27. G. H. Golub and C. F. Van Loan, *Matrix Computations*, JHU Press, Baltimore, Maryland (2012).
28. W. Osten, "Some considerations on the statistical error analysis in holographic interferometry with application to an optimized interferometer," *J. Mod. Opt.* **32**(7), 827–838 (1985).
29. F. Mendoza Santoyo, M. C. Shellabear, and J. R. Tyrer, "Whole field in-plane vibration analysis using pulsed phase-stepped ESPI," *Appl. Opt.* **30**(7), 717–721 (1991).
30. E. Harrington et al., "Automatic acquisition and processing of large sets of holographic measurements in medical research," *Opt. Meas. Model. Metrol.* **5**, 219–228 (2011).
31. G. Earl et al., "Reflectance transformation imaging systems for ancient documentary artefacts," in *Electronic Visualization and the Arts BCS* BCS, London (2011).
32. T. J. Atherton and D. J. Kerbyson, "Size invariant circle detection," *Image Vis. Comput.* **17**(11), 795–803 (1999).
33. A. Asundi and V. R. Singh, "Amplitude and phase analysis in digital dynamic holography," *Opt. Lett.* **31**(16), 2420–2422 (2006).
34. C. J. Taylor and D. J. Kriegman, "Minimization on the Lie group SO (3) and related manifolds," Yale University, New Haven, Connecticut (1994).

Morteza Khaleghi is a PhD candidate in mechanical engineering at Worcester Polytechnic Institute, Worcester, Massachusetts. His research interests include biomedical imaging and developments of optical and nondestructive metrology systems.

Cosme Furlong is an associate professor of mechanical engineering at Worcester Polytechnic Institute, Worcester, Massachusetts, working in mechanics, optical metrology, and nanoengineering science and technology.

Mike Ravicz is an associate scientist and biomechanical engineer at Massachusetts Eye and Ear Infirmary, Boston, Massachusetts, exploring the mechanics and acoustics of the external, middle, and inner ear as well as working in signal processing and noise and vibration control.

Jeffrey Tao Cheng is an instructor in otology and laryngology at Massachusetts Eye and Ear Infirmary, Boston, Massachusetts, working on middle-ear mechanics and ear tissue biomechanics through measurements and modeling.

John J. Rosowski is a professor of otology and laryngology, and also of health sciences and technology, working in acoustics and mechanics of the external, middle, and inner ear, with an interest in comparative middle and external ear structure and function.